Cellulose (2017) 24:5101–5115
DOI 10.1007/s10570-017-1434-3

ORIGINAL PAPER

Behavior of cellobiose in iron-containing solutions: towards a better understanding of the dominant mechanism of degradation of cellulosic paper by iron gall inks

Alice Gimat · Anne-Laurence Dupont · Hélène Lauron-Pernot · Sabrina Paris · Véronique Rouchon · Pascale Massiani

Received: 4 April 2017 / Accepted: 2 August 2017 / Published online: 22 August 2017

Abstract Cellobiose, a dimer of glucose wearing a glycosidic bond as in cellulose, was used as model molecule to understand the chemical degradation pathways taking place in iron gall inks impregnated papers. Experiments were carried out in liquid phase at 80 °C to study the effects of pH and of the presence of iron and oxygen on the cleavage of the glycosidic bond. Capillary electrophoresis was used to quantitatively follow the cellobiose degradation and the formation of glucose. Attenuated total reflectance infrared spectroscopy of freeze-dried samples was done to identify the presence of secondary products of reaction. UV–Visible spectroscopy allowed monitoring the iron(II) and iron(III) contents as a function of time and pH. The data reveal that the simultaneous presence of iron and oxygen enhances the degradation of cellobiose. Nevertheless, even if some oxidation of the sugar molecules occurs, the predominant pathway of cellobiose decomposition is found to be acid-catalyzed hydrolysis due to the high acidity of the medium generated from the oxidation and precipitation of iron.

Keywords Cellobiose · Paper corrosion · Iron gall ink · pH · Oxidation · Acid-catalyzed hydrolysis

A. Gimat · A.-L. Dupont · S. Paris · V. Rouchon
Centre de Recherche sur la Conservation (CRC, USR 3224), Sorbonne Universités, Muséum National d'Histoire Naturelle, Ministère de la Culture et de la Communication, CNRS, CP21, 36 rue Geoffroy-Saint-Hilaire, 75005 Paris, France

A. Gimat · H. Lauron-Pernot · P. Massiani (✉)
Laboratoire de Réactivité de Surface (LRS), Sorbonne Universités, UPMC Univ Paris 06, CNRS, UMR 7197, 4 Place Jussieu, 75005 Paris, France
e-mail: pascale.massiani@upmc.fr

Introduction

Iron gall inks (IGIs) are made of gall nut extracts (rich in gallic acid) and iron(II) salts (such as iron(II) sulphate). In the presence of oxygen, the mixture of these two components produces a dark iron(III)/tannin precipitate characteristic of the ink color (Krekel 1999; Wunderlich et al. 1991; Ponce et al. 2016). Gum Arabic is usually added as a binder. Under certain conditions, IGIs can significantly damage the cellulosic paper substrate on which they are deposited, causing browning and loss of mechanical properties (Reissland 2000). This degradation proceeds first by diffusion of ink components around the ink lines (usually under high humidity conditions), followed by chemical reactions provoking paper browning and embrittlement.

Paper degradation has motivated numerous mechanistic studies. It is currently attributed to concurrence between acid-catalyzed hydrolysis and oxidation pathways, both provoking chain scissions (Kolar and Strlic 2006). In acidic medium, it is usually admitted

that acid-catalyzed hydrolysis is predominant while the oxidation reaction would be a secondary pathway (Zou et al. 1996a, b; Pork and Teygeler 2000). However, this scenario should be reconsidered in the case of papers impregnated with IGIs in view of the following observations:

1. There is no doubt that iron gall inks are acidic (pH values between 2 and 4) and thus likely to induce acid-catalyzed hydrolysis of cellulose. Nevertheless, this degradation pathway could no longer prevail in the presence of iron which rich chemistry allows envisioning oxidative degradation routes;
2. The presence of oxygen was shown to be a key factor for chain cleavage in IGI impregnated acidic papers, leading to fast depolymerization measurable at ambient temperature (Rouchon et al. 2011);
3. This depolymerization, still in the presence of oxygen, was found to be several orders of magnitude faster in acidic IGI impregnated papers than in acidic iron-free papers (Rouchon et al. 2016), revealing an effect of iron as well;
4. As proposed in the 1990s (Koppenol 1993), Fenton-like reactions could occur in these systems, involving oxidation of iron(II) into iron(III) and formation of highly reactive hydroxyl radicals ($HO^{\cdot}$). These radicals were indeed detected in iron-impregnated papers previously deacidified to reach a neutral to mildly alkaline pH range (between 6.5 and 8 (Selih et al. 2007)) in which (1) acid-catalyzed hydrolysis is not expected and (2) chain scissions rather take place through oxidative routes, mostly through β-alkoxy elimination reactions occurring on the oxidized cellulose. Hydroxyl radicals were similarly sought in acidic (non deacidified) IGI impregnated papers (pH 3–4) but they always remained below or close to the limit of detection; when detected, their negligible amounts were moreover of little relevance to account for paper degradation (Gimat et al. 2016). Conversely, Reactive Oxygen Species (ROS) distinct from hydroxyl radicals were formed, as deduced from Electron Paramagnetic Resonance spectroscopic experiments done in solution in the presence of a non-specific spin-trap (Gimat et al. 2016). This revealed the existence of some oxidative process, even if the precise nature of the ROS and their possible role in cellulose chains scissions remained unclear;
5. Most historical IGIs recipes involve a large excess of iron compared to gallic acid (Neevel 1995). Hence, iron not involved in the iron gall ink precipitate is free to interact with the surrounding components, for instance by binding with neighbor sulfates and sugars or through its oxidation or reduction by gallic acid (Powell and Taylor 1982; Burgaud et al. 2010).

All above considerations directly raise the questions addressed in this work (1) of the precise effects of oxygen and iron towards degradation of acidic IGI impregnated papers and (2) of the predominant mechanism involved between acid-catalyzed hydrolysis and oxidation.

A difficulty in modeling corrosion of paper by IGIs lies in the fact that the degradation process is not restricted to chemical aspects but also includes physical ones. Indeed, the paper and the ink are usually designed so that the ink line lies on the paper surface without significant penetration. In this case, the manuscript generally ages normally because the interaction between the ink and the cellulose is limited to a few fibers at the surface of the sheet. Yet, ancient manuscripts might have been exposed to high humidity during their lifetime, which enhances the possibility of diffusions of acidic components and of soluble iron in the paper. Even if these migrations obey physical mechanisms that are beyond the scope of this article, they may strongly impact the chemical degradation by increasing the amount of cellulosic material in contact with the migrating compounds. This process is uncontrolled, making the interpretation of chemical data more complex. Moreover, the distribution of the ink components within the paper is substantially heterogeneous (Rouchon and Bernard 2015). Hence, the use of paper is not appropriate to achieve a homogeneous distribution of reactants, as required for a proper modeling of chemical events, and liquid samples are to this respect more relevant.

To simplify the system, cellobiose (or β-D-glucopyranosyl(1→4)D-glucopyranose) was selected as a model molecule to substitute cellulose. It is the structural unit of cellulose, has one β-1,4 glycosidic bond and is soluble in water. Its degradation was studied in solution, in the presence or absence of iron, at two different pH (mildly or strongly acidic medium)

and under aerobic (O_2) or anaerobic (Ar) conditions. For each cellobiose molecule, the cleavage of the glycosidic bond is expected to lead to two glucose units. This was monitored by capillary electrophoresis, a technique that allowed separating and quantifying simultaneously cellobiose and glucose. The samples were analyzed by FTIR spectroscopy after sample freeze-drying to characterize eventual newly formed chemical groups. In addition, Fe^{2+} and Fe^{3+} concentrations were measured by UV–Vis spectroscopy to characterize the chemistry of iron in the solutions.

Experimental

Solution samples

Different types of parent aqueous solutions were first prepared, referred to as Acid (sulfuric acid solution obtained from H_2SO_4 Sigma-Aldrich, 95.0%), Fe_2 (iron(II) sulfate heptahydrate solution obtained from $Fe^{II}SO_4{\cdot}7H_2O$ Sigma, 99.0%) and Fe_3 (iron(III) sulfate pentahydrate solution obtained from $Fe_2^{III}(SO_4)_3{\cdot}7H_2O$ Accros organics, 99.0%). The ink (referred to as Ink) consisted of a combination of Fe_2 and gallic acid monohydrate (Sigma, 97.5%) with a molar ratio Fe:gallic acid of 3, identical to the ratio identified in a previous study as appropriate to represent historical iron gall inks (Rouchon et al. 2011). The initial concentration of iron in all iron containing solutions was 41.9 mmol L^{-1}. Note that Gum Arabic, a main component of IGIs, was not added to the model ink, because its effect consists mainly in being a physical barrier preventing diffusion phenomena (Remazeilles et al. 2004, 2005).

The samples were prepared by dissolving 3 g of D(+)-cellobiose (99.0% Sigma Aldrich, supplier specification Fe < 5 ppm) in 34 mL of one of the above mentioned solutions. This was done under stirring in an experimental set-up made of a reflux condenser attached to a triple neck round bottom flask that allowed homogeneous heating (silicon oil bath) and gas sparging directly into the solution (Fig. 1). The cellobiose concentration (259 mmol L^{-1}) was chosen so as to reach a constant molar ratio iron:cellobiose of 0.16 in all iron containing samples. This ratio matches iron rich original manuscripts thereby an iron concentration in the paper of 26 mg g^{-1} (or approx. 2×10^{18} atoms cm^{-2} assuming a paper grammage close to 70 g m^{-2}) (Remazeilles et al. 2001).

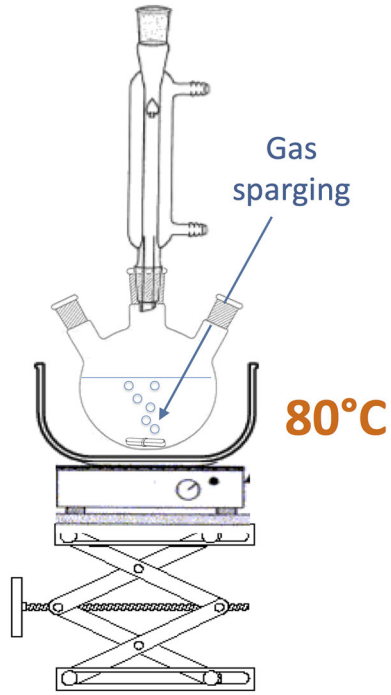

Fig. 1 Experimental setup for aging of diluted cellobiose solution samples

All prepared solutions were heated at a temperature of 80 °C found appropriate to accelerate degradation and thus make the experiments feasible in a suitable time scale (few days). Oxygen-rich conditions (referred to as O_2) were obtained by oxygen bubbling (25 mL min^{-1}) so as to ensure oxygen saturation in the solutions. Conversely, oxygen-free conditions (referred to as Ar) were obtained with argon bubbling (25 mL min^{-1}) and using de-aerated water that had been placed under argon bubbling for at least 1 h prior to the preparation of the solution.

Table 1 lists the names of the samples and details the initial concentrations in Fe_2, Fe_3, Ink and Acid as well as the nature of the sparging gas. The pH was 1.6 ± 0.2 (3.6 ± 0.2, respectively) in the acid solutions prepared with 25 mmol L^{-1} (0.32 mmol L^{-1}, respectively) of sulfuric acid. In addition, a blank sample, referred to as Blank_O_2, was made in aerobic conditions by dissolving 3 g of cellobiose in 34 mL of purified water (Milli-Q, Millipore).

Table 1 List of all prepared aqueous solution samples (initial cellobiose concentration: 259 mmol L^{-1})

Sample	Initial concentrations in solutions (mmol L^{-1})			Sparging gas	pH after 1 day	Color after 1 day	Cellobiose conversion
	Sulfuric acid	Iron	Gallic acid				
$Acid_{1.6}$_Ar	25	–	–	Ar	1.5	Colorless	Yes
$Acid_{1.6}$_O_2	25	–	–	O_2	1.6	Colorless	Yes
Fe_2_$Acid_{1.6}$_Ar	25	41.9	–	Ar	1.8	Colorless	Yes
Fe_2_O_2	–	41.9	–	O_2	1.6	Orange	Yes
$Acid_{3.6}$_Ar	0.32	–	–	Ar	3.6	Colorless	No
$Acid_{3.6}$_O_2	0.32	–	–	O_2	3.6	Colorless	No
Fe_2_Ar	–	41.9	–	Ar	3.5	Colorless	No
Fe_2_$NaOH_{3.6}$_O_2[a]	–	41.9	–	O_2	3.7	Orange/brown	No
Fe_3_O_2	–	41.9	–	O_2	1.6	Orange	Yes
Ink_O_2	–	41.9	14	O_2	2	Blue/Brown	Yes
Blank_O_2	–	–	–	O_2	5.5	Colorless	No

[a] Regular addition of a 0.1 mol L^{-1} NaOH solution along aging to maintain pH at 3.6

Aging methodology

The solutions were kept during 10 days under continuous stirring and gas bubbling, and Milli-Q water was added from time to time to replace the water lost by evaporation. Two aliquots of 3 mL were taken after an aging time t of 0, 1, 3, 7 and 10 days (as well as 15 days for the Fe_2–O_2 sample) for analysis:

- the first aliquot was cooled to ambient temperature in an ice-water bath and used for pH measurements and, if necessary, iron quantification;
- the second aliquot was frozen at −20 °C then stored until sugar analyses carried out by capillary electrophoresis (quantitative determination of cellobiose and glucose concentrations, done for all samples) and by infrared spectroscopy in ATR mode (done on few selected samples to identify specific carbohydrates).

In what follows, the initial samples will be called fresh samples while the others will be considered as aged ones.

Capillary electrophoresis

In order to analyze sugars by capillary electrophoresis, a derivatization reaction (Dahlman et al. 2000; Sjöberg et al. 2004; Dupont et al. 2007) was done between the sugar and an UV-absorbing molecule (4-aminobenzoic acid ethyl ester, also called benzocaine or ABEE, Sigma) allowing UV detection. The reagent solution consisted in a 100 mg mL^{-1} ABEE and 100 mg mL^{-1} acetic acid (99.6%, Carlo Erba Reagents) in methanol. 1 mL of this reagent solution was mixed with 10 mg of sodium cyanoborohydride (95%, Aldrich) in conical bottom vials, then with 1 mL of the sample solution that had been previously diluted (by a factor 51) in deionized water. After heating for 1 h at 80 °C, the unreacted ABEE was precipitated by adding 3 mL of aborate buffer at pH 8.6 (450 mmol L^{-1} boric acid (99.79%, Fisher Chemicals) and sodium hydroxide (Fisher Chemicals) in Milli-Q water). Each vial was finally vortexed and cooled to room temperature and the precipitate was removed by filtration with a Chromafil filter (0.20 µm PTFE, Macherey–Nagel).

The capillary electrophoresis system (P/ACE™ MDQ, Beckman Coulter) was equipped with a Photodiode Array Detector (PDA). The method (Dupont et al. 2007) used a fused silica capillary (20 µm internal diameter and 40 cm effective length) rinsed before each analysis (flushing with 0.1 mol L^{-1} NaOH for 1 min and then with deionized water for 1.5 min) and conditioned for 3 min with the running borate buffer (450 mmol L^{-1} boric acid, pH 9.9). The injection was made in hydrodynamic mode by applying a pressure of 0.5 psi for 20 s. The separation voltage was 28 kV applied to the anodic end and the resulting current was 17 µA. The run was carried out at 20 °C and the data collection rate was set at 4 Hz. The derivatized sugars were detected at 305 nm, with a bandwidth of 30 nm. They were identified according

to their migration time compared to the model compounds. After analysis, the capillary was rinsed for 2 min with deionized water.

The "32 Karat 5.0" software (Beckman Coulter) was used for data acquisition, calibration and quantification. Sugars concentrations in the diluted solutions were determined and cellobiose (C_t) and glucose (G_t) concentrations at each aging time t were calculated based on a calibration curve made for each sugar. The calibration for cellobiose was done in the range 0.210–14.6 mmol L^{-1} and yielded a linear plot with $R^2 = 0.9995$. Limits of detection (LOD) and of quantification (LOQ) were 0.210 and 0.700 mmol L^{-1}, respectively. For glucose, the calibration was done within the range 0.19–5.55 mmol L^{-1}, yielding to a linear plot with $R^2 = 0.9982$ and to LOD and LOQ of 0.190 and 0.650 mmol L^{-1}, respectively. Normalized cellobiose concentration (N_t) and glucose yield (R_t) at time t were finally deduced using the formulas $N_t = C_t/C_0$ and $R_t = G_t/2C_0$, where C_0 is the initial cellobiose concentration.

Since iron has a high ability to form precipitates that may block small capillaries, it was also important to verify that the presence of iron/ink did not hinder the measurements. To this end, fresh samples with and without iron/ink were analyzed. Similar concentrations were obtained which meant that the filtration step performed prior to the measurements to remove the excess ABEE was sufficient to also remove potentially formed iron particles.

Spectroscopic measurements

Cellobiose degradation was also monitored by infrared spectroscopy on selected samples, using a Nicolet 6700 spectrometer (Thermo scientific) equipped with a diamond crystal allowing recording of spectra in single reflection ATR (attenuated total reflectance) mode (ATR-FTIR). Before the experiments, the aliquots were freeze-dried for 48 h with a Cryos-55 (Cryotec) apparatus. Infrared spectra were collected within the range 500–4000 cm^{-1}, with a resolution of 4 cm^{-1} (average of 128 scans). All spectra were background subtracted and normalized with respect to the C-H stretching vibration at 2897 cm^{-1}.

In addition, UV–Visible spectroscopy was used to measure Fe^{2+} and Fe^{3+} concentrations in the sample solutions, using chelating agents able to form specific colored complexes. The agent was 2,2-bipyridyl (99.5%, Merck) for Fe^{2+} determination [stability constants of 17 (Thompsen and Mottola 1984; Fresenius and Schneider 1965)]: the reactant solution was prepared at a concentration of 0.45 mmol L^{-1}, after completion to 50 mL with a 25 mmol L^{-1} phosphate buffer prepared with sodium phosphate monobasic anhydrous (99%, Merck) and sodium phosphate dibasic anhydrous (99%, Merck). The pH of the final solution was 6. For Fe^{3+} determination (stability constant of 2.3 (Charlot 1961; Najib and Hayder 2011), the chelating agent was potassium thiocyanate, added at a concentration of 0.85 mol L^{-1} in a 4 mmol L^{-1} sulfuric acid solution. The pH of the final solution was 2. In both cases, the fresh aliquots (from section "Aging methodology") were placed into 50 mL flasks that contained the reactants for iron dosage. The spectra were recorded between 350 and 600 nm with a V-570 JASCO UV–Visible spectrometer. Quantifications were done at the absorption maxima (523 and 479 nm for Fe^{2+} and Fe^{3+}, respectively) identified from calibration curves previously established in the range 0–0.1 mmol L^{-1} and with $R^2 = 0.9996$ for both Fe^{2+} and Fe^{3+}.

Results

Impact of oxygen and Fe_2 on cellobiose degradation

Cellobiose degradation was first monitored in the solutions prepared with iron (full lines in Fig. 2a, b). For $Fe_2\_O_2$ aged in aerobic conditions, the normalized cellobiose concentration N_t decreased regularly with aging time until reaching 80% cellobiose conversion after 10 days (full squares, Fig. 2a), showing that cellobiose was not stable in the medium containing both Fe^{2+} ions and oxygen. This agrees with a previous viscometry study where Fe^{2+} impregnated cellulosic papers suffered 50% loss of degree of polymerization when they were kept in aerobic conditions: in this work, the depolymerization occurred within a few days at ambient temperature and a few hours at 80 °C, but it was significantly reduced when dry O_2 atmosphere was replaced by dry N_2 (Rouchon et al. 2011, Rouchon et al. 2016). Similarly, cellobiose was much less degraded in the present experiments when Ar was used instead of O_2 as bubbling gas (sample Fe_2_Ar, empty squares, Fig. 2b). This analogy in terms of effect of oxygen

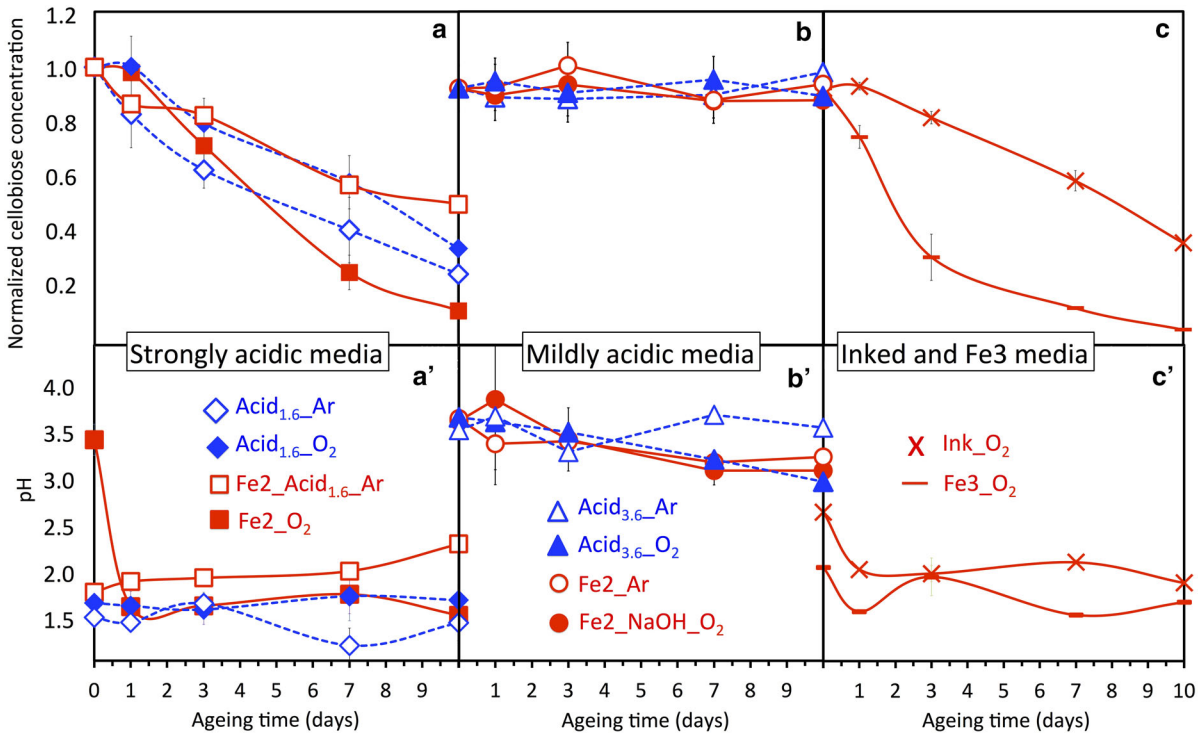

Fig. 2 Evolution with aging time of the (**a**–**c**) normalized cellobiose concentrations and (**a′**–**c′**) pH of solutions for samples with iron (*full lines*) and without iron (*dotted lines*). Aerobic and anaerobic conditions are represented by full (O_2) and empty (Ar) markers, respectively

between cellobiose conversion (this work) and cellulose depolymerization in paper (previous work) confirms that oxygen plays a role in the degradation.

Since the only difference with respect to preparation between Fe_2_O_2 and Fe_2_Ar was the nature of the bubbling gas, a blank test was performed to verify if oxygen alone (no iron in the solution) could initiate the decomposition of cellobiose. To this end, a control solution free of iron was prepared (Blank_O_2 sample) and left to age under oxygen bubbling at 80 °C. After 10 days, cellobiose concentration was unchanged demonstrating that neither oxygen alone nor the applied temperature of 80 °C promoted, by themselves, cellobiose degradation. It was rather the combination of oxygen with Fe_2 that provoked cellobiose conversion in the Fe_2_O_2 sample.

Correlation between pH and cellobiose degradation

It is well established that iron(II) in presence of oxygen is prone to oxidation, resulting in the formation of iron(III). The latter is also known to behave as a Lewis acid, releasing protons through formation of the $Fe^{III}(OH)^{2+}$ and $Fe^{III}(OH)_2^{+}$ hydrated iron complexes with respective pKa values of 2.4 and 4.7. Both phenomena may have impacted the pH of above solutions and pH appears therefore as an important parameter to follow versus time, as well.

The pH was the same (equal to 3.6) in the fresh Fe_2_Ar and Fe_2_O_2 samples, in agreement with their identical initial chemical composition. Nevertheless, while this value remained almost constant in Fe_2_Ar (slight decrease from 3.6 to 3.3 after 10 days, empty circles, Fig. 2b′), it rapidly dropped to about 1.6 within a few hours in Fe_2_O_2 and then stabilized at this value until the end of the experiment (full squares, Fig. 2a′). Hence, pH was indeed strongly impacted by the oxygenation (aerobic or anaerobic) conditions, which could account for the distinct levels of cellobiose degradation observed in Fe_2_Ar and Fe_2_O_2.

In order to confirm this effect, complementary experiments were carried out which consisted in preparing a set of solutions with or without iron at

two pH values: the pH of 3.6 (characteristic of a mildly acidic medium) corresponds to usually reported values for iron impregnated papers while the pH of 1.6 (typical of strongly acidic medium) was chosen with reference to the above strong pH drop in $Fe_2\_O_2$ during the first stage of the experiment. In this new set of solutions, the pH was the natural one (left to naturally fall without adjustment), except for two solutions in which pH was either maintained at the initial value of 3.6 by regularly adding NaOH (sample $Fe_2\_NaOH\_O_2$) or artificially decreased down to 1.6 by adding an appropriate volume of H_2SO_4 (sample $Fe_2\_Acid_{1.6}\_Ar$) (Table 1).

Before going further, it is worth recalling that kinetics of acid-catalyzed hydrolysis decrease with decreasing protons concentration (Zou et al. 1996b). The absence of cellobiose conversion in the series of mildly acidic samples at pH 3.6 (Fig. 2b) is therefore consistent with limited hydrolysis process at this stable pH (Fig. 2b′), and this is independent on iron presence ($Fe_2\_NaOH\_O_2$ and Fe_2_Ar) or absence ($Acid_{3.6}\_O_2$ and $Acid_{3.6}\_Ar$). Conversely, faster acid-catalyzed hydrolysis is expected at very low pH, in line with the cellobiose conversion observed in all samples at pH 1.6 (Fig. 2a). At this low pH and after a long duration of 10 days, it reached 75% which is similar to what was reported for cellobiose degradation after 2 h at 80 °C at higher sulphuric acid concentration [0.5 mol L^{-1} (Kwon et al. 2012)]. By comparison, it was 40% after 5 h at 150 °C under Ar (100 psi) (Deng et al. 2011).

Nevertheless, even if observed in all acidic solutions (Fig. 2a, a′), the cellobiose degradation at low pH occurred more or less rapidly depending on the sample: it was similar in $Fe_2\_O_2$ (full squares) and $Acid_{1.6}\_Ar$ (empty diamonds) but lower in both $Fe_2\_Acid_{1.6}\_Ar$ (empty squares) and $Acid_{1.6}\_O_2$ (full diamonds). The slightly lower pH in $Acid_{1.6}\_Ar$ could explain the higher degradation in this sample compared to $Fe_2\_Acid_{1.6}\_Ar$ (also placed under argon). However, there is no pH difference between $Fe_2\_O_2$ and $Acid_{1.6}\_O_2$ after one day of aging (full marks, Fig. 2a′) and the faster cellobiose degradation in the $Fe_2\_O_2$ solution should then come from another—possibly oxidative—degradation pathway besides acid-catalyzed hydrolysis.

Occurrence and impact of iron oxidation

More insight on the possible oxidative mechanism occurring in the presence of oxygen and Fe_2 was obtained by following the Fe^{2+} and Fe^{3+} concentrations in $Fe_2\_O_2$ as a function of aging time. A rapid decrease of the Fe^{2+} concentration was observed during the first day of the experiment (Fig. 3a), in the same timeframe as the decrease of pH (Fig. 2a′). Simultaneously, Fe^{3+} was formed in concentrations (maximum at 4.2 mmol L^{-1}) that remained largely below those of the lost Fe^{2+} (up to 18.8 mmol L^{-1}). This resulted in a total iron concentration in solution ($Fe_{aq.tot}$) about 50% below the initial one (41.9 mmol L^{-1}) at the end of the experiment, consistent with the progressive appearance of an orange precipitate later identified as goethite (XRD data, Fig. 3c).

This can be modeled by a two-step reaction consisting of the oxidation of a large proportion (until approx. 60%) of Fe^{2+} (reaction 1), then the precipitation of the formed ferric ions into oxide-hydroxides (reaction 2). The superimposition of these two steps leads to an overall acidification of the solution (reaction 3):

$$4\,Fe^{2+} + O_2 + 4\,H^+ \rightarrow 4\,Fe^{3+} + 2H_2O \quad (1)$$

$$4\,Fe^{3+} + 8\,H_2O \rightarrow 4\,FeOOH + 12\,H^+ \quad (2)$$

$$4\,Fe^{2+} + O_2 + 6\,H_2O + \rightarrow 4\,FeOOH + 8\,H^+ \quad (3)$$

The significant formation of protons in reaction (3) can explain the fast pH decrease observed in $Fe_2\_O_2$. The occurrence of such acidification process was further supported by performing an additional experiment where pH was followed in an aerobic iron(II) solution (same as $Fe_2\_O_2$) without cellobiose. Again, a fast pH drop from 3.6 to 1.6 took place within one day, together with the formation of an orange-brown precipitate. This confirms the important impact of iron oxidation and precipitation towards acidification of the medium that, in turns, enhances acid-hydrolysis of cellobiose. It is worth adding that the Fe^{2+} concentration was on the contrary stable in the absence of oxygen (data not shown), demonstrating again the effect of oxygen.

To complete these results, two additional aerobic samples were prepared in the same conditions as for $Fe_2\_O_2$, but using either Fe_3 ($Fe_3\_O_2$ sample) or Ink

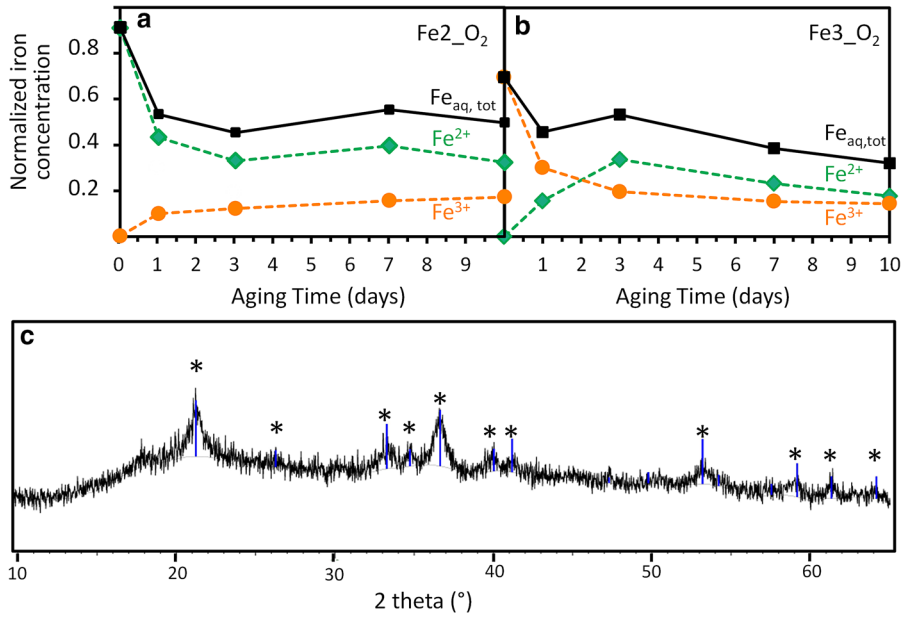

Fig. 3 Fe^{2+}, Fe^{3+} and total aqueous $Fe_{aq.tot}$ concentrations (normalized with respect to initial concentration) measured by UV–Vis spectroscopy in samples **a** $Fe_2\_O_2$ and **b** $Fe_3\_O_2$. **c** The iron missing in solution ($Fe_{aq.tot}$ below 1) is due to precipitation as goethite (*) as identified by X-ray diffraction

(Ink_O_2 sample) as starting iron component. Cellobiose degradation took place in both cases, but it was slightly slower in Ink_O_2 (crosses, Fig. 2c) than in $Fe_2\_O_2$ (full squares, Fig. 2a), probably due to the higher pH range for the former (from initially 2.6 down to 2 during aging, Fig. 2c′). On the contrary, cellobiose degradation was faster in $Fe_3\_O_2$ (straight lines, Fig. 2c), which is consistent with the pH as low as 2 in the fresh solution due the higher acidity of Fe^{3+} ions compared to Fe^{2+}. It is worth recalling that the acidification of the medium containing both iron and gallic acid (Ink_O_2 sample) could come additionally from the formation of the iron gall ink precipitate, which according to a recent study (Ponce et al. 2016) induces a deprotonation of the gallic acid phenolic groups and thus protons release.

Surprisingly, some proportion of Fe^{2+} was also formed during aging of the $Fe_3\_O_2$ sample (Fig. 3b), indicating that this solution contained a reducing species able to transform part of Fe^{3+} into Fe^2 ions. In view of the compounds present in solution, this species should be related to sugar molecules present in the system. This reinforces the hypothesis that a redox mechanism involving cellobiose (or its degradation products) could take place as secondary degradation mechanism.

Glucose quantification

In addition to cellobiose conversion, capillary electrophoresis provided quantitative data on glucose formation. The glucose yields with aging time (R_t, full lines) and the yield of total sugars normalized concentration ($R_t + N_t$, dotted lines) are shown in Fig. 4 for all samples where cellobiose conversion was detected. Strictly based on glycosidic bond breaking, one cellobiose molecule should lead to the formation of two glucose molecules. Then, the total sugars normalized concentration should be 1.

Such value was obtained within experimental precision during aging of both acidic iron-free samples ($Acid_{1.6}\_Ar$ and $Acid_{1.6}\_O_2$), independently on the presence or absence oxygen (dotted lineswith enmpty and full squares, Fig. 4a). This cellobiose conversion into almost exclusively glucose is consistent with a degradation pathway based on acid-catalyzed hydrolysis. Such pathway could also lead to smaller compounds such as formaldehyde or formic acid as already reported for diluted solutions of cellulose placed at temperatures above 180°C (Kupiainen 2012), but these compounds were not detected in our case. Similar observations were done for the anaerobic $Fe2\_Acid_{1.6}\_Ar$ sample (empty circles, Fig. 4a),

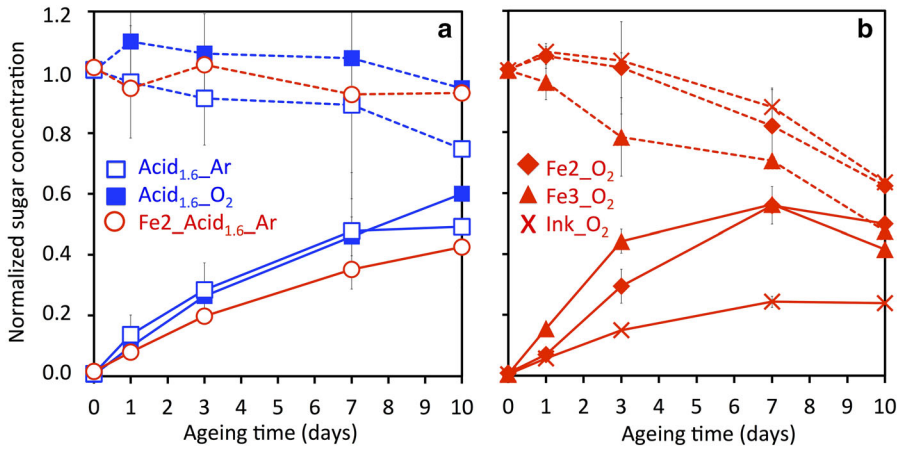

Fig. 4 Evolution with aging time of glucose production (Rt, *full lines*) and of total sugar concentrations (Rt + Nt, *dotted lines*) in the strongly acidic solutions (pH 1.6). The left and right parts correspond to solutions (**a**) where glucose was almost exclusively formed as products or (**b**) where side products distinct from glucose were also present (Rt + Nt lower than 1). Aerobic and anaerobic conditions are represented by full (O_2) and empty (Ar) markers, respectively

suggesting again the prevalence of an acid-catalyzed hydrolysis degradation route in this acidic sample containing iron but not oxygen.

Contrarily, the total sugars (cellobiose + glucose) normalized concentration were no longer equal to 1 in all aerobic solutions containing iron, and they progressively decreased after three days of aging down to 0.5 or 0.6 depending on the sample (dotted lines, Fig. 4b). Hence, degradation of either cellobiose or glucose into secondary products occurred at a significant level. This degradation was not directly linked to a change of pH, neither to the Fe^{2+} or Fe^{3+} concentrations, since all these parameters were constant during the same period of time (from 3 to 10 days, Figs. 2 and 3). This demonstrates that degradation routes other than glycosidic bond scissions exist in presence of both oxygen and iron (whichever the iron oxidation state).

Spectroscopic investigation of oxidation products

Infrared spectroscopy in ATR-FTIR mode was used to monitor the molecular changes and the possibly formed oxidation products during aging. It was performed on samples in their solid form obtained by freeze-drying to remove water which intense absorption bands would jeopardize the interpretation of spectra.

Figure 5 shows a typical cellobiose spectrum obtained with fresh $Fe_2\_O_2$ as representative example. Several groups of bands are observed, which all agree with wavenumber ranges classically reported in the literature for cellobiose (Table 2). For the present study, the most relevant information expected from cellobiose degradation and from secondary products formation would have been in the fingerprint region (1500–650 cm^{-1}), which detailed interpretation faced however two difficulties. First, in spite of using conditions recommended in the literature (Heljo et al. 2012; Nireesha et al. 2013), the freeze-dried cellobiose was not fully amorphous and it had a high propensity to recrystallize upon hydration (Heljo et al. 2012). This was not easy to control, even by keeping the samples in a dessicator, and it strongly impacted all infrared bands (including in the region of interest). Changes with sample aging were therefore not easy to analyze properly. Secondly, some of the samples contained iron sulfate (coming from samples preparation) which absorption bands superimpose those of cellobiose in the 970–1100 cm^{-1} region that is characteristic of both S–O asymmetric stretching vibrations of $FeSO_4$ and of C–OH streching vibrations of cellobiose.

Due to these limitations, the detection of spectral changes was done only the 1850–1650 cm^{-1} region where water absorption and C=O stretching bands are distinct from those of the sugar molecules and of their related degradation products. Figure 5b, c compare the spectral evolution in this region for the $Acid_{1.6}\_O_2$ and $Fe_2\_O_2$ samples, respectively. The band at 1641 cm^{-1} corresponds to water remaining after

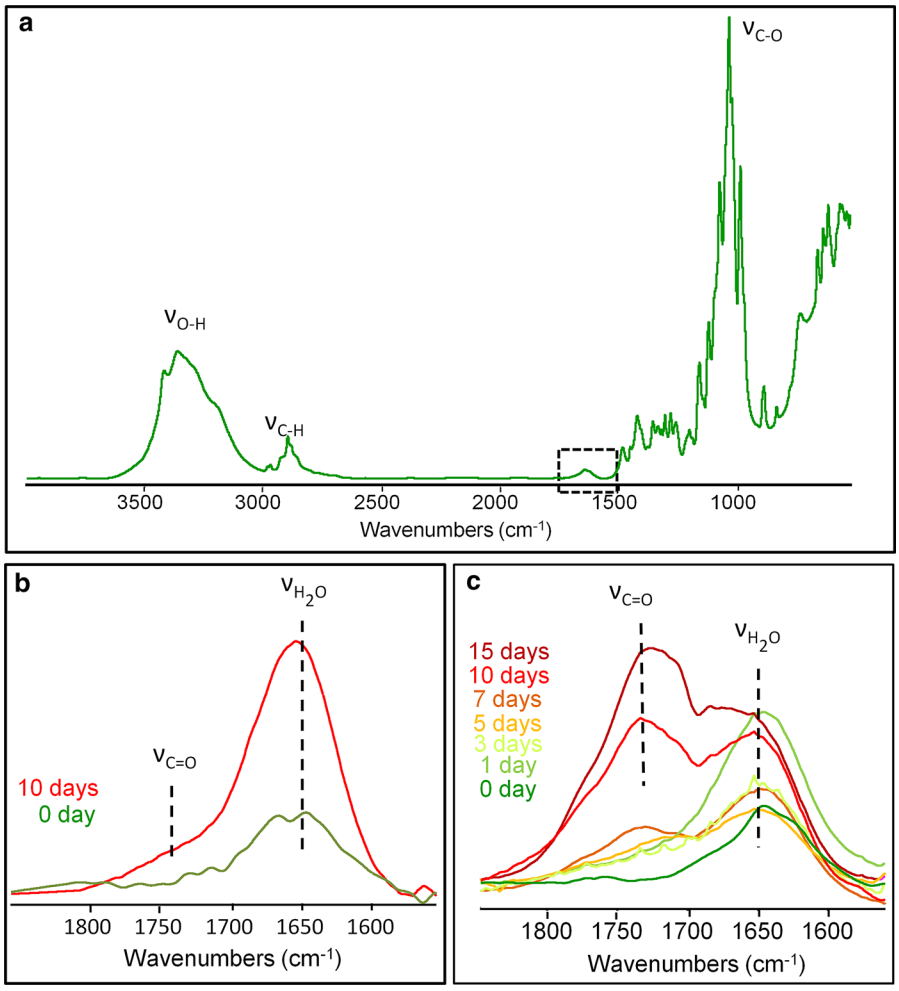

Fig. 5 **a** Typical infrared spectrum of cellobiose obtained after freeze-drying the fresh Acid_O_2_1.6 solution; enlarged spectra in the 1550–1850 cm^{-1} range (*dashed square* in the main figure) showing the evolution with aging for samples **b** Acid_O_2_1.6 and **c** Fe_2_O_2_1.6

freeze-drying and eventually re-adsorbed in spite of the efforts to limit rehydration. This band tended to increase with aging, revealing a higher hydration state of the aged freeze-dried samples. This seems to indicate a higher sensitivity of more degraded samples to rehydration.

A small broad shoulder is also visible, after aging of $Acid_{1.6}$_O_2, centered near 1730 cm^{-1} (Fig. 5b). It could be tempting to assign it to aldehyde end-groups resulting from glycosidic bond cleavage, but this hypothesis was ruled out for two reasons. Firstly, the band is slightly shifted compared to the 1718 cm^{-1} value previously reported for aldose and ketose systems undergoing epimerization (Parker 2012). Secondly, the band was not observed before aging while the sample should already contain a considerable number of such end-groups. Hence, this signal might indicate some (although very limited) formation of C=O bonds by weak oxidation in aerated $Acid_{1.6}$_O_2 as discussed in the last section.

On the iron-containing Fe_2_O_2 sample, the absorption around 1730 cm^{-1} is still present and its intensity strongly increases after aging (by more than 4 times for the 15 days aged samples compared to the 5 days one). Moreover the bands in this region (1850–1550 cm^{-1}) are broad and asymmetric, indicating several contributions. For each aging time, this part of the spectra was deconvoluted in a series of Gaussian–Lorentzian, as illustrated in Fig. 6a for the sample aged 15 days, which allowed to discriminate seven distinct components. Three of them (1621, 1641 and 1682 cm^{-1}) were initially present. The band at 1641 cm^{-1} is typical of the O–H bending vibration modes of adsorbed water (Fan et al. 2012; Faure 2013)

Table 2 main reported infrared absorption bands for cellobiose (Socrates 2001; Nikonenko et al. 2000)

Wavenumbers (cm^{-1})	Attribution
3421/3364/3327/3285/3187	O–H stretching (H bounding)
2982/2971	C–H stretching of aliphatic groups
2929/2917	C–H asymmetric stretching
2897	C–H stretching
2884	C–H stretching
2863	C–H symmetric stretching
1454	C–C–H deformations (scissoring)
1426	C–C–H deformations or C–OH
1359/1337/1309	O–H deformation (alcohol I or II)
1260	C–H deformations (out of plane) or C–OH cyclic
1204	O–H deformation (alcohol I or II)
1163/1145	C–O–C glycosidic linkage
1123	C–O stretching ou 6-o-cycle
1098	C–OH stretching (alcohol II) or cyclic C–O
1079/1040	C–OH stretching (alcohol I or II) or cyclic C–O
1027	C–OH stretching (alcohol I) or cyclic C–O
989/975	C–O–C glycosidic linkage
895/890/836	C–H deformation
640	O–H deformation

but the attribution of the tow other bands is less straightforward. Even if the one at 1682 cm^{-1} is within the range of conjugated C=O, this attribution seems unlikely since this band was already present in the fresh (in principle C=O free) cellobiose solution. An alternative could be that the 1621 and 1682 cm^{-1} bands come from water with different degrees of hydrogen bonding (low and high H-bonding, respectively) and/or from water interacting with metal ions as already reported for other solids (Lin et al. 2017). Besides, the band at 1621 cm^{-1} is within the 1560–1628 cm^{-1} range, which is typical of iron oxalates (Calvini and Silveira 2008; Ferrer and Sistach 2005). This attribution seems however unlikely in the present case due to the presence of this band before aging.

Four other bands progressively appeared with aging. Those at 1705 and 1662 cm^{-1} could not be assigned with certainty, but they interestingly matched values calculated for the formation of two carboxylic acid functions on cellopentaose (Lojewska et al. 2006). They are also compatible with aldehyde end group formation

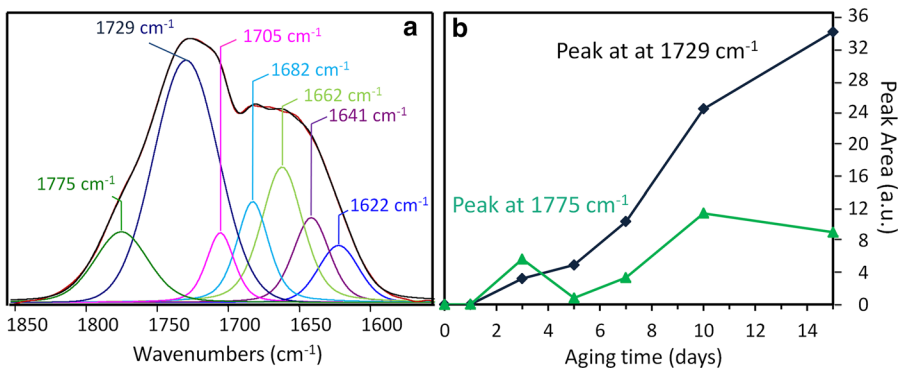

Fig. 6 **a** Deconvolution of the infrared signal between 1550 and 1850 cm^{-1} for the $Fe_2\_O_2\_1.6$ sample aged 15 days and **b** evolution with aging time of the area of the infrared components at 1729 and 1775 cm^{-1}

and water, respectively. Those at 1729 and 1775 cm^{-1} are typical of the C=O stretching mode of different functional groups, such as aldehyde, ketone, carboxylic acids or lactones (Socrates 2001). On paper, the band at 1729 cm^{-1} was previously mainly attributed to carboxyl groups, the participation of aldehyde end groups being negligible for cellulose (Lojewska et al. 2006). More generally on carbohydrates, carboxylic acid groups absorb in the range 1730–1740 cm^{-1}, ketone or aldehyde end groups of open-ring sugars around 1718 cm^{-1}, lactones between 1760 cm^{-1} and 1726 cm^{-1} (for aldono-1,5-lactone) and 1790 cm^{-1} and 1765 cm^{-1} (for aldono-1,4-lactone) and ester between 1748 cm^{-1} and 1724 cm^{-1} (for example 1727 cm^{-1} on cellobiose octoacetate).

The deconvolution of the 1700–1800 cm^{-1} region in the series of aged $Fe_2\_O_2$ samples allowed measuring the peak area for each individual component and following their evolution with aging time. Amongst the seven components, only the two bands at 1729 and 1775 cm^{-1} regularly increased with time (Fig. 6b), evidencing C=O formation during aging at a much higher level than in the previous iron-free solution, consistent with the accentuated higher degradation of cellobiose evidenced by capillary electrophoresis.

Discussion on the effect of oxygen on iron gall inked paper degradation

All above data on cellobiose degradation in the presence of iron and oxygen provide a clearer picture of the reaction pathways involved in the depolymerization of acidic IGI impregnated papers. If simultaneously present, iron and oxygen accelerate the degradation of cellulose and this trend, observed earlier on inked papers (Rouchon et al. 2011), is confirmed here using cellobiose as model molecule for cellulose.

The present work goes further and demonstrates that the impact of oxygen is mostly related to an acidification of the medium through iron(II) oxidation to iron(III), followed by iron(III) precipitation. Without gallic acid ($Fe_2\_O_2$ sample), this process is relatively fast (less than one day in the conditions of the experiments) and it induces simultaneously (1) a pH decrease, (2) a color change of the solution (from colorless to orange) and (3) the precipitation of goethite. Interestingly, such color change, characteristic of an oxidation of iron(II) to iron(III) was also observed in $Fe_2\_NaOH\_O_2$ in which cellobiose was not degraded because pH was kept at 3.6 by addition of NaOH. Thus, pH appears to be the main impacting factor in the degradation.

In all mildly acidic media, cellobiose conversion was negligible regardless of the presence or absence of iron and/or oxygen. Conversely, it occurred in all samples at pH 1.6, moreover accentuated in the presence of both iron and oxygen. Not only glucose (formed by glycosidic bond breaking) but also secondary products of degradation (evidenced by the progressive appearance of C=O infrared bands at 1729 and 1775 cm^{-1}) were obtained. The newly formed C=O groups could arise through oxidation of cellobiose or glucose, but they could result as well from isomerization of glucose to fructose and subsequent dehydration, as has been observed in acidic medium (Popoff and Theander 1976). This leads to the formation of hydroxymethylfurfural (HMF), humins and possibly levulinic acid and formic acid (Kwon et al. 2012). All these new molecules bear C=O groups that might account for the increase of both above-mentioned IR absorption bands. The fact that formation of such C=O bearing dehydration by-products was not detected in $Acid_{1.6}\_Ar$ (no signal) and was seen at a very small extent in $Acid_{1.6}\_O_2$ (broad weak signal around 1730 cm^{-1}) agrees with the observation of Kwon et al. (Kwon et al. 2012) who reported that cellobiose hydrolysis is easier than glucose dehydration, the former process being therefore favored. Conversely, the significant increase of the C=O bands with aging for the $Fe_2\_O_2$ sample attest of the occurrence of some cellobiose oxidation in addition to hydrolysis, similarly to what was reported for cellulose in an iron free medium (Bouchard et al. 1989). In our case, it is thought that iron participates to the oxidation through (at least partially) radicalar mechanism, as deduced from a previous study in which we demonstrated by ESR spectroscopy that reactive oxygen species (ROS) were produced in solutions when iron(II) lixiviated from impregnated paper samples was oxidized to iron(III) (Gimat et al. 2016). It is also worth adding that the formation of electron-attracting groups such as carbonyls in the neighborhood of the glycosidic oxygen was found to favor acid hydrolysis explaining the higher hydrolysis rate in wood pulp in comparison to cotton (Krässig 1993).

The predominance of the acid-catalyzed hydrolysis degradation pathway in $Fe_2\_O_2$ is also consistent with previous kinetics measurements done on an acidic IGI impregnated paper exposed to air and to 50% relative humidity. Indeed, the depolymerization rate on this paper was several orders of magnitude higher than on iron-free papers with similar pH (3–4) and the activation energy (E_a) value of the process was equal to 97 ± 2 $kJ.mol^{-1}$, close to reported E_a values for acid-catalyzed hydrolysis (100–115 $kJ.mol^{-1}$) (Rouchon et al. 2016). Nevertheless, a new question arises when considering the pH of this acidic paper that is within the usual range for acid papers but is close to the pH of our mildly acidic (stable) cellobiose solutions and far above that at 1.6 of the acidic (degraded) ones. This apparent discrepancy finds a convincing explanation in the fact that pH of paper samples is usually measured in water extracts using standard protocols (TAPPI T 509 om-02). It is thus an average value of the protons released by the paper in solution. Two papers with similar average pH but with different distributions of acidic compounds at the microscopic level in the fibers may in all likelihood behave differently. In the case of IGI impregnated papers, the formation of the iron(III) precipitate may induce a strongly acidic environment locally, favorable to acid hydrolysis, while similar amounts of protons distributed more homogeneously in the fibers would have a much lower impact. This scenario would explain why no cellobiose degradation was observed at 80 °C in $Fe_2\_NaOH\_O_2$ that was maintained at pH 3.6, while chain scissions were measured at ambient temperature on IGI impregnated papers with similar apparent pH (average value). Getting a better insight into these aspects requires investigating paper samples at the nano-scale. This can be done using techniques that allow mapping the IGI or iron distribution within paper fibers. Scanning Transmission X-ray Microscopy (STXM) is one such technique and proved to be useful for this purpose (Rouchon and Bernard 2015). This investigation will be the purpose of the following work.

Conclusion

In this work, cellobiose was used as a model molecule to study the mechanism leading to glycosidic bond breaking in cellulose in presence of iron and oxygen. This approach appeared relevant since the effect of oxygen and iron was qualitatively similar in cellobiose solutions (this work) and on IGI impregnated paper samples (previous publications). In both systems the combined presence of iron and oxygen was highly detrimental and rapidly led to glycosidic bond cleavage.

The choice of working in solution, a homogeneous system, enabled to study the chemistry taking place and circumvent the physical aspects related to the migration of ink components in paper fibers. It showed that the most deleterious effect of oxygen and iron was operating through a fast acidification of the medium consecutive to iron oxidation, leading to acid-catalyzed hydrolysis of cellobiose. Cellobiose oxidation also occurred, to some extent, leading to some formation of C=O bonds which can weaken the glycosidic bond (so-called "weak links") and make it more prone to cleavage by acid hydrolysis. The impact of cellulose oxidation on chain scission is thus synergetic, as the glycosidic bond cleavage was mainly driven by the pH of the solutions. Nevertheless, the main degradation mechanism was clearly acid-catalyzed hydrolysis.

Despite the pH dependence of chain scissions, extrapolating the behavior of cellobiose solutions to a solid substrate such as paper is not straightforward. Indeed the pH of a paper is usually measured on aqueous extracts. This gives an average value of all the acidic components that can be extracted from the paper, but does not take into account the eventual heterogeneous distribution of the components within the fibers that can induce local pH differences. Therefore, at similar pH, the behavior of a paper may not be comparable with the behavior of solutions. On an IGI impregnated paper, local spots of iron may induce very low pH at the microscopic/nanoscopic scale. This point needs confirmation by nanoscale observations, but could explain why IGI papers at pH 3–4 undergo strong depolymerization while cellobiose solutions at similar pH remain unaffected.

Acknowledgments We acknowledge the French state funds managed by the ANR within the "Investissements d'Avenir" program (reference ANR-11-IDEX-0004-02) for financial support within the framework of the Cluster of Excellence MATISSE. We also thank the French "Ile de France" region (DIM OxyMORE program) for the acquisition of an environmental climate chamber. We are grateful for V. Losinho (LRS)'s help with the experimental set-up.

References

Bouchard J, Abatzoglou N, Chornet E, Overend RP (1989) Characterization of depolymerized cellulosic residues. Wood Sci Technol 23:343–355. doi:10.1007/BF00353250

Burgaud C, Rouchon V, Wattiaux A, Bleton J, Sabot R, Refait P (2010) Determination of the Fe(II)/Fe(III) ratio in iron gall inks by potentiometry: a preliminary study. J Electroanal Chem 650:16–23

Calvini P, Silveira M (2008) FTIR analysis of naturally aged $FeCl_3$ and $CuCl_2$-doped cellulose papers. E-Preserv Sci 5:1–8

Charlot G (1961) Dosages colorimétriques des éléments minéraux: principes et méthodes. Masson, pp 396

Dahlman O, Jacobs A, Lijenberg A, Al Olssson (2000) Analysis of carbohydrates in wood and pulps employing enzymatic hydrolysis and subsequent capillary zone electrophoresis. J Chromatogr A 891:157–174. doi:10.1016/S0021-9673(00)00619-1

Deng W, Lobo R, Setthapun W, Christensen ST, Elam JW, Marshall CL (2011) Oxidative hydrolysis of cellobiose to glucose. Catal Lett 141(4):498–506. doi:10.1007/s10562-010-0532-8

Dupont AL, Egasse C, Morin A, Vasseur F (2007) Comprehensive characterisation of cellulose- and lignocellulose degradation products in aged papers: capillary zone electrophoresis of low-molar mass organic acids, carbohydrates, and aromatic lignin derivatives. Carbohyd Polym 68:1–16. doi:10.1016/j.carbpol.2006.07.005

Fan M, Dai D, Huang B. (2012) Fourier transform infrared spectroscopy for natural fibres. In: Salih S Fourier transform–materials analysis, p 260. ISBN: 978-953-51-0594-7

Faure AM (2013) Hydroxyl radical mediated degradation of cereal eta-glucan. PhD thesis, ETH ZURICH, Zurich

Ferrer N, Sistach MC (2005) Characterization by FTIR spectroscopy of ink components in ancient manuscripts. Restaurator 26(2):105–117

Fresenius W, Schneider W (1965) Determination of iron (II) and total iron with 2,2′-dipyridyl in mineral waters. Reduction of iron (III) with ascorbic acid Translation from: Zeitschrift fur Analytische Chemie 209(2):340–341

Gimat A, Kasneryk V, Dupont AL, Paris S, Averseng F, Fournier J, Massiani P, Rouchon V (2016) Investigating the DMPO-formate spin trapping method for the study of paper iron gall ink corrosion. New J Chem 40:9098–9110. doi:10.1039/C6NJ01480A

Heljo VP, Nordberg A, Tenho M, Virtanen T, Jouppila K, Salonen J, Maunu SL, Juppo AM (2012) The effect of water plasticization on the molecular mobility and crystallization tendency of amorphous disaccharides. Pharm Res 29:2684–2697. doi:10.1007/s11095-011-0658-4

Kolar J, Strilic M (2006) Iron gall inks: on manufacture, characterisation, degradation and stabilisation. National and University Library, Ljubljana

Koppenol WH (1993) The centennial of the fenton reaction. Free Radic Biol Med 15:645–651. doi:10.1016/0891-5849(93)90168-T

Krässig HA (1993) Cellulose. Structure, accessibility and reactivity. Gordon and Breach Sci. Pub, Singapore, p 189

Krekel C (1999) Chemische Struktur historischer Eisengallustinten. In: Banik G (ed.) Tintenfrassschäden und ihre Behandlunh, Stuttgart, Germany, pp 25–37

Kupiainen L (2012) PhD dissertation, Dilute acid catalysed hydrolysis of cellulose—extension to formic acid, Acta Universitatis Ouluensis. C, Technica. ISBN: 978-952-62-0002-6

Kwon Y, Kleijn S, Schouten K, Koper M (2012) Cellobiose hydrolysis and decomposition by electrochemical generation of acid and hydroxyl radicals. Chemsuschem 5:1935–1943. doi:10.1002/cssc.201200250

Lin L, Cornu D, Mounir-Daou M, Domingos C, Herledan V, Krafft JM, Laugel G, Millot Y, Lauron-Pernot H (2017) Role of water on the activity of magnesium silicate for transesterification reactions. ChemCatChem 9(12):2399–2407. doi:10.1002/cctc.201700139

Łojewska J, Lubańska A, Miśkowiec P, Łojewski T, Proniewicz LM (2006) FTIR in situ transmission studies on the kinetics of paper degradation via hydrolytic and oxidative reaction paths. Appl Phys A 83:597–603. doi:10.1007/s00339-006-3529-9

Najib FM, Hayder OI (2011) Study of stoichiometry of ferric thiocyanate complex for analytical purposes including F^- determination. Iraqi Natl J Chem 42:135–155

Neevel JG (1995) Phytate: a potential conservation agent for the treatment of ink corrosion caused by iron gall inks. Restaurator 16(3):143

Nikonenko NA, Buslov DK, Sushko NI, Zhbankov RG (2000) Investigation of stretching vibrations of glycosidic linkages in disaccharides and polysaccharides with use of IR spectra deconvolution. Biopolymers 57:257–262

Nireesha GR, Divya L, Sowmya C, Venkateshan N, Niranjan BM, Lavakumar V (2013) Lyophilization/freeze drying—an review. Int J Novel Trends Pharm Sci 3:87–93

Parker F (2012) Applications of infrared spectroscopy in biochemistry, biology, and medicine. Springer, Berlin, p. 612. ISBN: 978-1-4684-1872-9

Ponce A, Brostoff LB, Gibbons SK, Zavalij P, Viragh C, Hooper J, Alnemrat S, Gaskell KJ, Eichhorn B (2016) Elucidation of the Fe(III) gallate structure in historical iron gall ink. Anal Chem 88:5152–5158. doi:10.1021/acs.analchem.6b00088

Popoff T, Theander O (1976) Formation of aromatic compounds from carbohydrates. Part III. Reaction of D-glucose and D-fructose in slightly acidic, aqueous solution. Acta Chem Scand B30:397–402

Pork H, Teygeler R (2000) Preservation science survey: an overview of recent developments in research on the conservation of selected analog library and archival materials, chap 1. Council on Library and Information Resources publisher, Amsterdam. ISBN: 1-887334-80-7

Powell HKJ, Taylor MC (1982) Interactions of iron(II) and iron(III) with gallic acid and its homologues: a potentiometric and spectrophotometric study. Aust J Chem 35:739–756

Reissland B (2000) Visible progress of paper degradation caused by Iron Gall inks. In: Brown JAE (ed) The iron gall ink meeting. University of Northumbria, Newcastle upon Tyne, pp 67–72

Remazeilles C, Quillet V, Calligaro T, Claude Dran J, Pichon L, Salomon J (2001) PIXE elemental mapping on original

manuscripts with an external microbeam. Application to manuscripts damaged by iron-gall ink corrosion. Nuclear instruments and methods in physics research section B: beam interactions with materials and atoms. In: Seventh international conference on nuclear microprobe technology and applications 181:681–687. doi:10.1016/S0168-583X(01)00364-0

Remazeilles C, Rouchon-Quillet V, Bernard J (2004) Influence of gum arabic on iron gall ink corrosion. Part I: a laboratory samples study. Restaurator 25(4):220–232

Remazeilles C, Rouchon-Quillet V, Bernard J, Calligaro T, Claude Dran J, Pichon L, Salomon J, Eveno M (2005) Influence of gum arabic on iron-gall ink corrosion. Part II: observation and elemental analysis of originals. Restaurator 26(2):118–133

Rouchon V, Bernard S (2015) Mapping iron gall ink penetration within paper fibres using scanning transmission x-ray microscopy. J Anal Atomic Spectrosc 30(3):635–641. doi:10.1039/C4JA00358F

Rouchon V, Duranton M, Burgaud C, Pellizzi E, Lavédrine B, Janssens K, de Nolf W, Nuyts G, Vanmeert F, Hellemans K (2011) Room-temperature study of iron gall ink impregnated paper degradation under various oxygen and humidity conditions: time-dependent monitoring by viscosity and x-ray absorption near-edge spectrometry measurements. Anal Chem 83:2589–2597. doi:10.1021/ac1029242

Rouchon V, Belhadj O, Duranton M, Gimat A, Massiani P (2016) Application of arrhenius law to dp and zero-span tensile strength measurements taken on iron gall ink impregnated papers: relevance of artificial ageing protocols. Appl Phys A 122:773. doi:10.1007/s00339-016-0307-1

Selih VS, Strlic M, Kolar J, Pihlar B (2007) The role of transition metals in oxidative degradation of cellulose. Polym Degrad Stab 92:1476–1481

Sjöberg J, Adorjan I, Rosenau T, Kosma P (2004) An optimized CZE method for analysis of mono- and oligomeric aldose mixtures. Carbohyd Res 339:2037–2043. doi:10.1016/j.carres.2004.06.003

Socrates G (2001) Infrared and Raman characteristic group frequencies: tables and charts. Wiley, New York. Google-Books-ID: LDoAAjMnwEIC. ISBN: 978-0-470-09307-8

Thompsen JC, Mottola HA (1984) Kinetics of the complexation of iron(II) with ferrozine. Anal Chem 56:755–757. doi:10.1021/ac00268a037

Wunderlich CH, Weber R, Bergerhoff G (1991) Über Eisengallustinte. Zeitschrift Für Anorganische Und Allgemeine Chemie 598:371–376. doi:10.1002/zaac.19915980134

Zou X, Uesaka T, Gurnagul N (1996a) Prediction of paper permanence by accelerated aging I. Kinetic analysis of the aging process. Cellulose 3:243–267. doi:10.1007/BF02228805

Zou X, Uesaka T, Gurnagul N (1996b) Prediction of paper permanence by accelerated aging II. Comparison of the predictions with natural aging results. Cellulose 3:269–279. doi:10.1007/BF02228806